78-GT-172

an ASME publication

$3.00 PER COPY
$1.50 TO ASME MEMBERS
1.00 £ at Wembley

The Stability of an Asymmetric Rotor in Damped Supports

A. J. SMALLEY
Assistant Manager

J. M. TESSARZIK
Senior Development Engineer

R. H. BADGLEY
Manager

Machinery Dynamics Center,
Mechanical Technology Incorporated,
Latham, N. Y.

A general-purpose method of evaluating the stability of an asymmetric flexible rotor, mounted in symmetric damped bearings, is defined. This method evaluates the complex eigenvalues of the rotor system by solving the equations of motion in a rotating coordinate frame. The application of this method to a rotor mounted in tilting-pad bearings is demonstrated. The observed behavior of a number of different rotor configurations is compared with corresponding predictions of stability. For the configurations predicted to be unstable, a distinct and unnegotiable threshold of instability is encountered. The sharpness of this threshold is emphasized by careful balancing at speeds fractionally below the threshold. In a final configuration predicted to be marginally stable, lightly damped resonant behavior, negotiable by balancing, is encountered in the region of the first critical speed.

Contributed by the Gas Turbine Division of The American Society of Mechanical Engineers for presentation at the Gas Turbine Conference & Products Show, London, England, April 9-13, 1978. Manuscript received at ASME Headquarters December 27, 1977.

Copies will be available until January 1, 1979.

THE AMERICAN SOCIETY OF MECHANICAL ENGINEERS, UNITED ENGINEERING CENTER, 345 EAST 47th STREET, NEW YORK, N.Y. 10017

The Stability of an Asymmetric Rotor in Damped Supports

A. J. SMALLEY **J. M. TESSARZIK** **R. H. BADGLEY**

NOMENCLATURE

A = cross-sectional area of shaft, L^2
$\underline{\underline{B}}$ = bearing translational damping matrix, FTL^{-1}
B_{xx}, B_{xy} = direct and cross-coupling translational damping coefficient, FTL^{-1}
D_{xx}, D_{xy} = angular direct and cross-coupling damping coefficients, FTL
E = Young's modulus, FL^{-2}
f^+, f^- = frequencies (Hz) of the "half-power points" for a critical speed
f_n = resonant frequency, Hz
$(I_\xi)_n, (I_\eta)_n$ = transverse moments of inertia about ξ, η axes, L^4
J_{tn}, J_{pn} = transverse and polar moments of inertia at a station, L^4
$\underline{\underline{K}}$ = bearing translational stiffness matrix, FL^{-1}
ℓ_n = distance between station n and station n+1, L
M_n = concentrated mass at station n, M
M_{xn}, M_{yn} = bending moment at lower numbered side of station, FL
M_{xn}', M_{yn}' = bending moment at higher number side of station, FL
N = number of stations
S = complex eigenvalue, T^{-1}
$\underline{\underline{T}}$ = transfer matrix
t = time, T
V_{xn}, V_{yn} = shear forces at lower number side of station, F
V_{xn}', V_{yn}' = shear forces at higher numbered side of station, F
x_n = displacement in x-direction at station n, L
y_n = displacement in y-direction at station n, L
α = angle of rotor deflection in ξ plane; also shape factor for shear deformation
β = angle of rotor deflection in η plane
Δ = determinant of transfer matrix
Δp = determinant of transfer matrix with elements of p^{th} column replaced by their derivatives with respect to S
δ = log decrement
ξ^* = amplitude of displacement in ξ direction, L
ξ, η = rotating coordinate direction, L
Θ_n = angle of rotor deflection in fixed frame (x-z plane)
λ = real part of eigenvalue, T^{-1}
ϕ_n = angle of rotor deflection in fixed frame (y-z plane)
Ω = rotational angular velocity, T^{-1}
ω = imaginary part of eigenvalue expressed in nonrotating frame, T^{-1}
ω^1 = imaginary part of eigenvalue expressed relative to rotating coordinate frame, T^{-1}

TERMINOLOGY

"Major Diameter" -- This is the diameter of the circular arc portion of the flattened section of shaft.

"Unstable Speed Range" -- This is the speed range over which the real part of the complex eigenvalue is predicted to be positive.

INTRODUCTION

Elastic asymmetry in a flexible rotor tends to induce instability when the rotor is run near to its pair of first bending critical speeds. Smith (1)[1] recognized and analyzed the instability, as more recently have a number of workers, including Foote, Poritsky and Slade (2), and Hsu (3, 4). For the case of a rotor mounted

[1] Underlined numbers in parentheses designate References at end of paper.

symmetric bearings, an idealized Jeffcott model with damping applied directly to the central mass was analyzed by Bones and Hannam (5). Black (6) presents an elegant treatment of the case where both shaft and bearings are asymmetric.

As shown by workers in this field, it is possible to improve the stability of an asymmetric rotor by means of external damping at the supports. However, when the need arises to analyze a general multimass rotor and to establish necessary levels of damping, even with symmetric bearings, the available methods are either too simplified, or assume knowledge of mode shapes, natural frequencies, and modal damping ratios. They are thus often not practical for general use.

In the present paper, previous work on the subject is extended to provide a general method of analyzing a multimass flexible rotor, with flexural asymmetry, mounted in symmetric bearings. Because of the asymmetry, the equations of motion in stationary coordinates would have time-varying coefficients. The free vibration equations of the rotor are, therefore, solved in rotating coordinates, to yield the complex eigenvalues at any running speed. Extensive use is made of the work of Lund (7).

The method was applied to a rotor consisting of three masses mounted on a flexible shaft on which two flattened sections have been machined. Over a range of running speeds in the region of the first pair of shaft flexural critical speeds, the complex eigenvalues were evaluated for different degrees of asymmetry, and the conditions for stable and unstable operation in the speed range were established. Tests were run on this rotor with varying degrees of asymmetry, and the corresponding predictions of stability and instability were borne out.

Two significant contributions of the work presented are, first, the development and verification of a general purpose method of stability analysis and, secondly, the emphasis, by balancing, of the distinct difference between the characteristics of forced response vibration and those of self-excited vibration.

In the following sections, the analysis, its application, and the test results are presented.

ANALYSIS

The rotor is described analytically as a series of stations, at which concentrated mass, and transverse and polar moments of inertia may be located. At any station a bearing, represented by radial stiffness and damping coefficients, may also be located. The rotor stations are considered to be connected by massless elastic beams (fields) capable of deformation in both bending and shear. Each field can have principal section moduli which differ from each other, with the stipulation that all fields have common principal axes (ξ and η), which form a rotating coordinate frame.

In the development which follows, the transfer equations for a typical station (transfer matrix) are written, first in fixed coordinates, then in rotating coordinates. The field transfer equations are written directly in rotating coordinates. A general expression for the motion of the rotor is written in the form:

$$\xi = \mathrm{Re}\{\xi^* e^{St}\} \tag{1}$$

where

$$S = \lambda + i\omega' \tag{2}$$

and

$$\omega' = \omega - \Omega.$$

Here ξ, S are complex and all phase information is contained in ξ^*. The development is actually performed for the more general case of

$$\xi = \xi^* e^{St} \tag{3}$$

Similar equations can be written for the η direction. So we can write

$$\frac{d}{dt} = S \tag{4}$$

$$\frac{d^2}{dt^2} = S^2 \tag{5}$$

The equations are solved to yield those values of S at which the complex system determinant is zero -- the only conditions under which a free vibration can take place. The rotor is stable if λ, the real part of S, is negative, and unstable if λ is positive.

Station Equations of Motion

Fig. 1 illustrates the sign convention for shear force, bending moment, and translational and angular displacements in the x-z plane. θ is the rotation angle for z to x. In the y-z plane, a similar diagram would show ϕ as being the rotation angle from z to y.

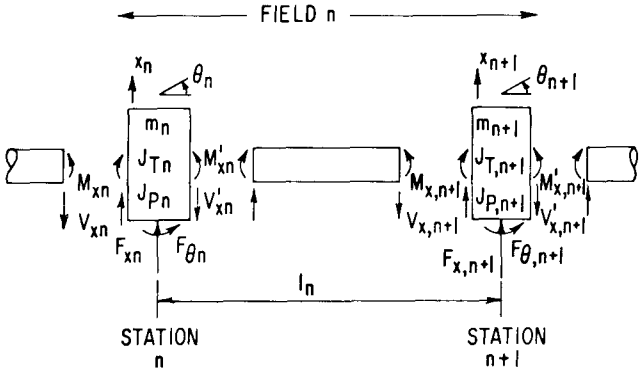

Fig. 1 Sign convention for radial displacement, angular displacement, bending moment, and shear force

If we consider that, in addition to inertia forces, any station may be acted upon by bearing forces, the forces acting at station n are related by:

$$\begin{Bmatrix} -V_{xn}' \\ -V_{yn}' \\ M_{xn}' \\ M_{yn}' \end{Bmatrix} = \begin{Bmatrix} -V_{xn} \\ -V_{yn} \\ M_{xn} \\ M_{yn} \end{Bmatrix} + \begin{Bmatrix} M_n \frac{d^2 x_n}{dt^2} \\ M_n \frac{d^2 y_n}{dt^2} \\ J_{tn} \frac{d^2 \theta_n}{dt^2} + \Omega J_{pn} \frac{d\phi_n}{dt} \\ J_{tn} \frac{d^2 \phi_n}{dt^2} - \Omega J_{pn} \frac{d\theta_n}{dt} \end{Bmatrix} + \underline{K} \begin{Bmatrix} x_n \\ y_n \\ \theta_n \\ \phi_n \end{Bmatrix} + \underline{B} \begin{Bmatrix} \frac{dx_n}{dt} \\ \frac{dy_n}{dt} \\ \frac{d\theta_n}{dt} \\ \frac{d\phi_n}{dt} \end{Bmatrix} \quad (6)$$

where $\underline{K}$, $\underline{B}$ are 4 x 4 isentropic bearing stiffness and damping matrices, with no coupling between translational and angular degrees of freedom.

Fig. 2 defines the coordinate directions (ξ, η, z) to be employed in a rotating plane, and their relation to the fixed (x, y, z) frame. In addition the relationships between angles (θ, ϕ) in the fixed frame and (α, β) in the rotating frame are illustrated.

To translate from the (x, y, z) system to the (ξ, η, z) system we must substitute into the station equations:

$$\begin{aligned} x &= \xi \cos \Omega t - \eta \sin \Omega t \\ y &= \xi \sin \Omega t + \eta \cos \Omega t \\ \theta &= \alpha \cos \Omega t - \beta \sin \Omega t \\ \phi &= \alpha \sin \Omega t + \beta \cos \Omega t \end{aligned}$$

and the result is:

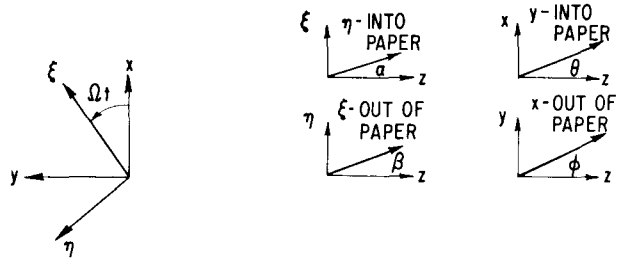

Fig. 2 Relationship between fixed and rotation coordinate frames

$$\begin{Bmatrix} -V_{\xi n}' \\ -V_{\eta n}' \\ M_{\xi n}' \\ M_{\eta n}' \end{Bmatrix} = \begin{Bmatrix} -V_{\xi n} \\ -V_{\eta n} \\ M_{\xi n} \\ M_{\eta n} \end{Bmatrix} + \begin{Bmatrix} M_n \frac{d^2 \xi_n}{dt^2} \\ M_n \frac{d^2 \eta_n}{dt^2} \\ J_{tn} \frac{d^2 \xi_n}{dt^2} + \Omega J_{pn} \frac{d\eta_n}{dt} \\ J_{tn} \frac{d^2 \eta_n}{dt^2} - \Omega J_{pn} \frac{d\xi_n}{dt} \end{Bmatrix} + \begin{Bmatrix} M_n(-\Omega^2 \xi_n - 2\Omega \frac{d\eta_n}{dt}) \\ M_n(\frac{2\,d\xi_n}{dt} - \Omega^2 \eta_n) \\ J_{tn}(-\Omega^2 \xi_n - 2\Omega \frac{d\eta_n}{dt}) + \Omega^2 J_{pn} \eta_n \\ J_{tn}(-\Omega^2 \eta_n + 2\Omega \frac{d\xi_n}{dt}) + \Omega^2 J_{pn} \xi_n \end{Bmatrix}$$

$$+ \underline{K} \begin{Bmatrix} \xi_n \\ \eta_n \\ \alpha_n \\ \beta_n \end{Bmatrix} + \underline{B} \begin{Bmatrix} \frac{d\xi_n}{dt} \\ \frac{d\eta_n}{dt} \\ \frac{d\alpha_n}{dt} \\ \frac{d\beta_n}{dt} \end{Bmatrix} + \underline{B}'' \begin{Bmatrix} \xi_n \\ \eta_n \\ \alpha_n \\ \beta_n \end{Bmatrix} \quad (8)$$

$$\text{where } B'' = \begin{bmatrix} B_{xy} & -B_{xx} & 0 & 0 \\ B_{xx} & B_{xy} & 0 & 0 \\ 0 & 0 & D_{xy} & -D_{xx} \\ 0 & 0 & D_{xx} & D_{xy} \end{bmatrix} \quad (9)$$

and B_{xx}, B_{xy} are direct and cross-coupling translational damping coefficients, D_{xx}, D_{xy} are the direct and cross-coupling angular damping coefficients in the bearing.

Finally, substituting

$$s = \frac{d}{dt}; \quad s^2 = \frac{d^2}{dt^2} \quad (10)$$

we get:

$$\begin{Bmatrix} -V_{\xi n}' \\ -V_{\eta n}' \\ M_{\xi n}' \\ M_{\eta n}' \end{Bmatrix} = \begin{Bmatrix} -V_{\xi n} \\ -V_{\eta n} \\ M_{\xi n} \\ M_{\eta n} \end{Bmatrix} + \begin{Bmatrix} M_n S^2 \xi_n \\ M_n S^2 \eta_n \\ J_{tn} S^2 \alpha_n + \Omega J_{pn} S\beta_n \\ J_{tn} S^2 \beta_n - J_{pn} S\alpha_n \end{Bmatrix} + \begin{Bmatrix} M_n(-\Omega^2 \xi_n - 2\Omega S\eta_n') \\ M_n(2\Omega S\xi_n - \Omega^2 \eta_n) \\ J_{tn}(-\Omega^2 \alpha_n - 2\Omega S\beta_n) + \Omega^2 J_{pn} \alpha_n \\ J_{tn}(-\Omega^2 \beta_n + 2\Omega S\alpha_n) + \Omega^2 J_{pn} \beta_n \end{Bmatrix} + (\underline{K} + S\underline{B} + \Omega \underline{B}') \begin{Bmatrix} \xi_n \\ \eta_n \\ \alpha_n \\ \beta_n \end{Bmatrix} \tag{11}$$

Field Equations

The elastic beams between stations are considered to have principal axes aligned with the $\xi - \eta$ coordinates as shown in Fig. 3.

Let $(I_\xi)_n$ be the second moment of area of the shaft between stations n and n+1, about an axis parallel to the ξ-axis. $(I_\eta)_n$ is the corresponding second moment of area about an axis parallel to the η-axis. The relationships between displacements, forces, and moments at the ends of the shaft section between stations n and n+1 are:

$$\xi_{n+1} = \xi_n + \ell_n \alpha_n + \frac{1}{(EI_\eta)_n} \left[\frac{\ell_n^2}{2} M_{\eta n}' + \left(\frac{\ell_n^3}{6} - \frac{(\ell E I_\eta)_n}{(\ell GA)_n} \right) V_{\xi n}' \right] \tag{12}$$

$$\eta_{n+1} = \eta_n + \ell_n \beta_n + \frac{1}{(EI_\xi)_n} \left[\frac{\ell_n^2}{2} M_{\eta n}' + \left(\frac{\ell_n^3}{6} - \frac{(\ell E I_\xi)_n}{(\ell GA)_n} \right) V_{\eta n}' \right] \tag{13}$$

$$\alpha_{n+1} = \alpha_n + \frac{1}{(E I_\xi)_n} \left[\ell_n M_{\xi n}' + \frac{\ell_n^2}{2} V_{\xi n}' \right] \tag{14}$$

$$\beta_{n+1} = \beta_n + \frac{1}{(E I_\eta)_n} \left[\ell_n M_{\eta n}' + \frac{\ell_n^2}{2} V_{\eta n}' \right] \tag{15}$$

$$M_{\xi, n+1} = M_{\xi n}' + \ell_n V_{\xi n}' \tag{16}$$

$$M_{\eta, n+1} = M_{\eta n}' + \ell_n V_{\eta n}' \tag{17}$$

$$V_{\xi, n+1} = V_{\xi n} \tag{18}$$

$$V_{\eta, n+1} = V_{\eta n} \tag{19}$$

Now, to implement the solution algorithm, a total of four calculations is performed, for an assumed value of S. Each of ξ_1, η_1, α_1, β_1 is, in turn, set to 1 while the others are maintained as zero. In addition, at the left-hand end (end 1) the free boundary conditions are imposed:

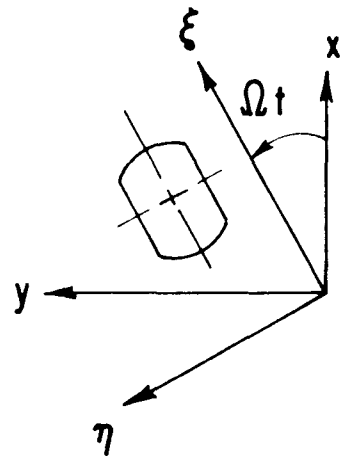

Fig. 3 Alignment of principal axes with rotating coordinate

$$M_{\xi 1} = M_{\eta 1} = V_{\xi 1} = V_{\eta 1} = 0 \tag{20}$$

The result of this calculation for the rotor may be expressed in matrix terms:

$$\begin{Bmatrix} M_{\xi N}' \\ M_{\eta N}' \\ V_{\xi N}' \\ V_{\eta n}' \end{Bmatrix} = \underline{\underline{T}} \begin{Bmatrix} \xi_1 \\ \eta_1 \\ \alpha_1 \\ \beta_1 \end{Bmatrix} \tag{21}$$

where $\underline{\underline{T}}$ is a square matrix, and N is the number of stations. To satisfy the free boundary condition at the right-hand end (station N) requires that Δ, the determinant of $\underline{\underline{T}}$ be zero, and the values of S which satisfy this condition are the complex eigenvalues from which the stability of the system can be determined.

An iterative solution, based on the generalized Newton Raphson method, is used to find these values of S. To implement this solution method, the determinant Δp of the matrix $\underline{\underline{T}}_p$ is required, in which the elements of the p^{th} column of $\underline{\underline{T}}$ have been replaced by their derivatives with respect to S. These derivatives are determined in a parallel operation to the determination of the element values. The starting values for all derivatives are zero:

$$\frac{d\xi_1}{ds} = \frac{d\eta_1}{ds} = \frac{d\alpha_1}{ds} = \frac{d\beta_1}{ds} = \frac{dM_{\xi 1}}{ds} = \frac{dM_{\eta 1}}{ds} = \frac{dV_{\xi 1}}{ds} = \frac{dV_{\eta 1}}{ds} = 0 \tag{22}$$

The field transfer relationships for the deriva-

tives are exactly the same as the relationships for the corresponding values (since they do not contain S). The station transfer relationships for the derivatives are different, however, as follows:

$$\begin{Bmatrix} -\frac{dV_{\xi n}}{ds} \\ -\frac{dV_{\eta n}}{ds} \\ \frac{dM_{\xi n}}{ds} \\ \frac{dM_{\eta n}}{ds} \end{Bmatrix} = \begin{Bmatrix} -\frac{dV_{\xi n}}{ds} \\ -\frac{dV_{\eta n}}{ds} \\ \frac{dM_{\xi n}}{ds} \\ \frac{dM_{\eta n}}{ds} \end{Bmatrix} + \begin{Bmatrix} S^2 M_n \frac{d\xi_n}{ds} - \Omega^2 M_n \frac{d\xi_n}{ds} - 2S\Omega M_n \frac{d\eta_n}{ds} \\ S^2 M_n \frac{d\eta_n}{ds} - \Omega^2 M_n \frac{d\eta_n}{ds} + 2S\Omega M_n \frac{d\xi_n}{ds} \\ S^2 J_{tn} \frac{d\alpha_n}{ds} - \Omega^2 J_{tn} \frac{d\alpha_n}{ds} - 2S\Omega J_{tn} \frac{d\beta_n}{ds} + S\Omega J_{pn} \frac{d\xi_n}{ds} + \Omega^2 J_{pn} \frac{d\alpha_n}{ds} \\ S^2 J_{tn} \frac{d\beta_n}{ds} - \Omega^2 J_{tn} \frac{d\beta_n}{ds} + 2S\Omega J_{tn} \frac{d\alpha_n}{ds} - S\Omega J_{pn} \frac{d\alpha_n}{ds} + \Omega^2 J_{pn} \frac{d\xi_n}{ds} \end{Bmatrix}$$

$$+ (\underline{K} + S\underline{B} + \Omega\underline{B}'') \begin{Bmatrix} \frac{d\xi_n}{ds} \\ \frac{d\eta_n}{ds} \\ \frac{d\alpha_n}{ds} \\ \frac{d\beta_n}{ds} \end{Bmatrix} + \underline{B} \begin{Bmatrix} \xi_n \\ \eta_n \\ \alpha_n \\ \beta_n \end{Bmatrix}$$

$$+ \begin{Bmatrix} 2SM_n \beta_n \\ 2SM_n \eta_n \\ 2SJ_{tn} \alpha_n + \Omega J_{pn} \beta_n \\ 2SJ_{tn} \beta_n - \Omega J_{pn} \alpha_n \end{Bmatrix} + \begin{Bmatrix} -2\Omega M_n \eta_n \\ +2\Omega M_n \beta_n \\ -2\Omega \beta_n J_{tn} \\ +2\Omega \alpha_n J_{tn} \end{Bmatrix} \qquad (23)$$

As shown by Reference (7), an iteration, which avoids convergence to roots already found is given by

$$S = S_o - \Delta_o / [(\frac{d\Delta}{dS})_o - \Delta_o \sum_{j=1}^{J} (1/(S_o - S_j))] \qquad (24)$$

where Δ_o, S_o are the current values of Δ and S in the iteration, J roots, S_j, have already been found, and $(d\Delta/dS)_o$ is the derivative of Δ with respect to S as determined by summing:

$$\frac{d\Delta}{dS} = \sum_{p=1}^{4} \Delta p \qquad (25)$$

Check of Analytical Method

The asymmetric rotor model of Bones and Hannam was used to check the analysis for a single mass supported on a massless, flexible shaft with external damping applied to the central mass. An exact check of the required damping value for the stability threshold was obtained, as shown in Appendix A.

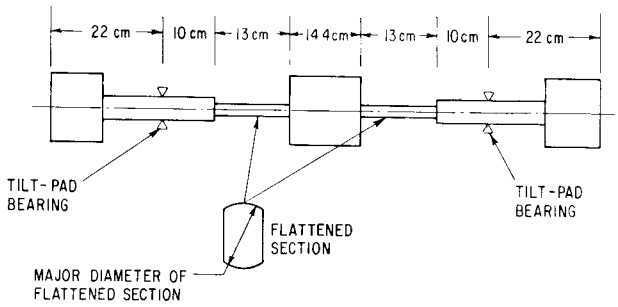

Fig. 4 Schematic of flattened shaft

APPLICATION

The test rotor to which the preceding analysis was applied is illustrated schematically in Fig. 4. It is approximately 105 cm long. Viewed from the side the rotor is nearly symmetrical, with a central mass and a mass at either end. Four-pad tilting-pad bearings are located 22 cm from either end. The bearings are loaded between the pads, so preserving isoelasticity in the vertical and horizontal directions. Between the bearings and the central mass are two 13-cm long sections of 6.51-cm original diameter in which equal flats 4.32 cm apart were initially machined to give a configuration both predicted and observed to be unstable. The analysis presented above was applied to this rotor with the objective of finding what reduction in the major diameter, "D," from 6.51 cm, would be necessary to stabilize the rotor, and what would be the influence of the intermediate values of diameter upon the state of stability of the rotor. (Major diameter refers to the diameter of the circular portion of the flattened sections, as illustrated in Figs. 4 and 5.)

If the rotor was unstable, when running speed was set close to or between the two first flexural critical speeds associated with the two principal axes, a pair of roots would be obtained, both of which would be synchronous (i.e., the imaginary part of S would be zero). For one root the real part would be negative and for the other the real part would be positive. The latter is an unstable root, since it indicates the rotor amplitude will grow rather than decay with time.

STRUCTURAL AUDIT CHECKLIST

Engineering Development Phase: Blade

Activity	Objective	Evaluation: Critical Parameter	Evaluation: Calculation Method	Evaluation: Criteria	Evaluation: Results	Evaluation: Error Band	Evaluation: Criteria Probability	Acceptability of Results: Yes	Acceptability of Results: No
Design and Analysis	Provide Adequate LCF Life and Creep/Stress Rupture Life	Airfoil to Platform Leading Edge/Trailing Edge Steady Stress Ratio	2D-3D Finite Element Analysis	Airfoil Leading Edge/Trailing Edge Stress Ratio					
		Airfoil Steady Stresses	Steady Stress Beam or Finite Element Analysis	____0.2% Creep Strength					
		Steady Stresses at Shroud to Airfoil Interface	Steady Stress Beam or Finite Element Analysis	____% Yield Strength ____1% Creep Strength					
		Shroud Bending Stress	Steady Stress Beam or Finite Element Analysis	____% Yield Strength ____ Stress Rupture Strength					
		Airfoil Platform Bending Stress	Steady Stress Beam Analysis	____% Yield Strength ____1% Creep ____Stress Rupture Strength					
		Blade Attachment Neck Tensile Stress	Steady Stress Beam Analysis or Hand Calculation	____1% Creep Strength					

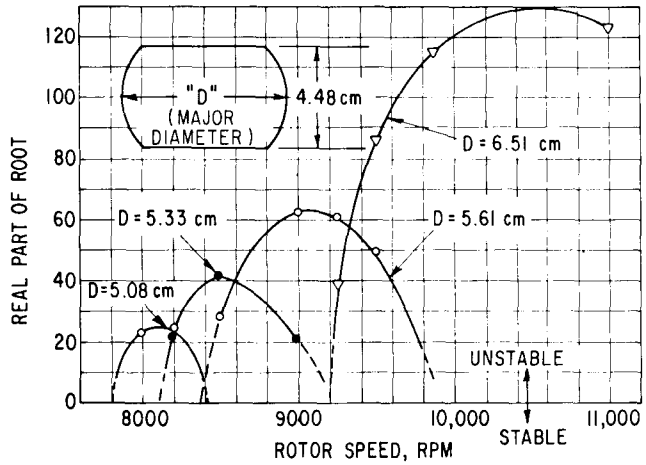

Fig. 5 Stability analysis -- real part of root versus speed for different major diameters

The nature of the results is illustrated graphically in Fig. 5, where the aforementioned positive real part is plotted against rotor speed for different values of major diameter (with constant distance maintained across the flats). For values of major diameter between 5 and 6.51 cm, an unstable speed range is indicated where the width of the speed range and the peak value of the real part of S increase with increasing major diameter. The indication is that a sufficient decrease in major diameter would shrink the height and width of the unstable speed range to zero. Interestingly, this dimensional change also shifts the speed range to lower speed values, since the overall flexibility of the shaft is increased.

In Fig. 6 the relationship between the maximum value of the real part of S and major diameter D is shown for two different mass distributions. In one case (the "original" rotor) the masses at either end are 4.94 kg. In the second case one of the masses has been reduced to 1.13 kg -- a change which changes the mode shape of the flexural critical speed slightly, increasing amplitude of the bearings and increasing the potential for damping. Clearly, the lighter end mass allows a stable rotor to be achieved with a larger major diameter, 4.80 cm as opposed to 4.62 cm. However, even 4.80 cm represents only a 7 percent difference between major diameter and the distance across the flats; surprisingly, such an apparently small asymmetry can destablize the rotor.

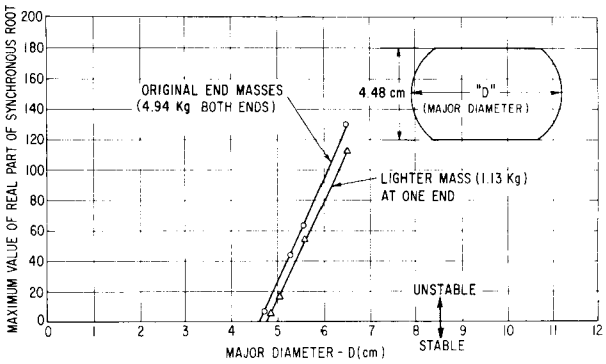

Fig. 6 Stability analysis -- real part of synchronous root versus major diameter (distance across flats = 4.48 cm)

TEST RESULTS

Four configurations of the test rotor shown in Fig. 4 were built and tested for stability near the first bending critical speed. These configurations are defined in Table 1 in terms of distance across flats, major diameter, and end masses. All but the last configuration were both predicted and observed to be unstable. The fourth configuration was predicted and observed to be stable although very lightly damped. Included in Table 1 are the threshold speeds for unstable vibration. In each case the predicted threshold speed is close to, but slightly higher than observed (by 200, 200 and 50 rpm, respectively). These results are considered an encouraging test of the prediction method.

Details on rotor and test bed construction, bearing configurations, and drive system may be obtained from Reference (9) where the same rotor with unmodified round sections had been used for balancing demonstrations for operation through three system critical speeds. For the tests described herein, bearing fluid viscosity, however, had been changed several times as noted. When bearing viscosity was increased beyond 5cS, bearing temperatures rose above the 5-7 C increase quoted in Reference (9). Displacements of the rotor under test were observed and recorded from five noncontacting displacement sensor pairs distributed along the length of the rotor.

The measured amplitudes for the third rotor configuration of Table 1 are presented as a function of speed in Fig. 7. Curve A shows the amplitudes with some initial unbalance present in the rotor and has a shape characteristic of resonant response to unbalance; the amplitude of response limits the closeness with which the critical speed may be approached. When most of the remaining rotor unbalance had been removed by in-place balancing, utilizing the Multiplane-Multispeed Balancing method, with data taken at approximately 8600 rpm, the rotor system critical speed could be approached much more closely with very low rotor amplitudes (Fig. 7, Curve B). However, at 8750 rpm there was a pronounced and sudden jump in amplitude, with a slope discontinuity not characteristic of resonant response. Further attempts to reduce amplitudes by balancing were unsuccessful even though the frequency of vibration was synchronous with rotor speed. Similar characteristics were observed for all of the unstable configurations presented in Table 1.

Bearing damping was found ineffective as a means to obtain stable rotor operation at the first critical speed. For example, with a rotor diameter at the flat sections of 5.72 cm, and the rotor in the best balanced condition (Fig. 7), an increase in bearing fluid viscosity from 5 cS to approximately 35 cS did not produce an improvement in rotor amplitudes at the first critical speed. Stable operation

Table 1 Rotor Configurations and Conditions

Rotor Configuration Number	Distance Across Flats (cm)	Major Diameter (cm)	End Masses (kg)	Condition (Predicted and Observed)	Predicted Threshold of Instability (rpm)	Observed Threshold of Instability (rpm)
1	4.48	6.51	Both 4.94	Unstable	9200	9000
2	4.48	6.51	One 4.94 One 1.13	Unstable	9500	9300
3	4.48	5.72	One 4.94 One 1.13	Unstable	8800	8750
4	4.48	4.80	One 4.94 One 1.13	Stable (lightly damped)	--	--

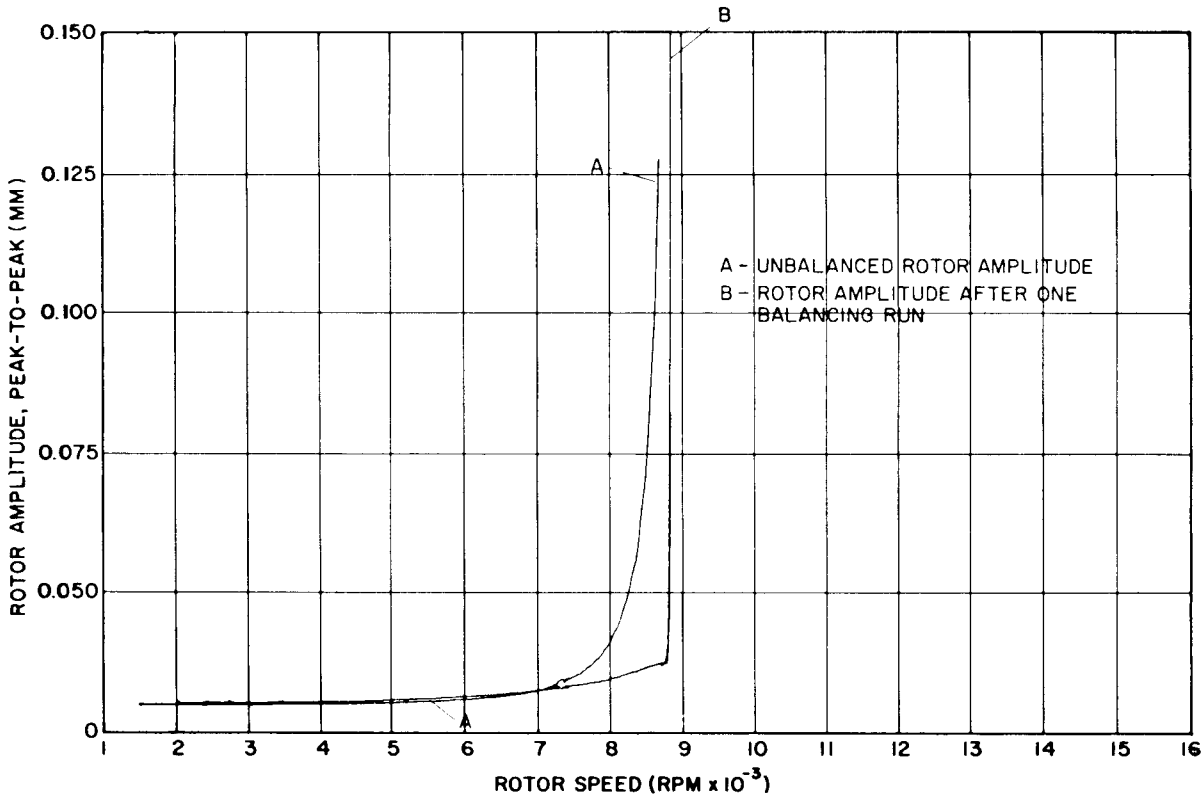

Fig. 7 Vertical rotor amplitudes at shaft center -- initial condition and after one balancing run by the least squares procedure (four vertical probes, rotor with 5.72 cm dia at flat sections)

at or above the first critical speed could not be achieved. Judged subjectively, the instability appeared to come in somewhat less violently for decreasing major diameters at the rotor flat sections and also for the rotor with one reduced end mass. Rapid fluctuations in orbit size ("breathing") which occurred just prior to amplitude explosion appeared to lessen as the predicted degree of stability was reduced.

By way of contrast, the measured amplitudes for the fourth configuration of Table 1 are presented as a function of speed in Fig. 8. In this configuration, the major diameter (4.80 cm) is only 7 percent greater than the distance across the flats (4.48 cm) and the configuration is predicted to be marginally stable. Curve A of Fig. 8 is for the rotor in its initial state of unbalance and Curves B and C show the results of successive balancing operations. Nowhere on the curves is there the pronounced and sudden increase in amplitudes of Fig. 7, Curve B, and the rotor could be readily balanced to operate at and above its first bending critical speed.

The rapid, but finite, amplitude buildup at the critical speed indicates a lightly damped system, thus confirming the prediction from the stability analysis presented in Table 1. As a measure of the system damping, the log decrement can be determined, approximately, from the shape of the response curve as follows:

$$\delta = \pi \left[\frac{f^+ - f^-}{f_n}\right] \qquad (26)$$

where f^+, f^- are the frequencies of the points at which the amplitude equals $(\sqrt{2}/2)$ times the peak amplitude and f_n is the resonant frequency (Hz).

The real part of the computed system eigenvalue (λ) can be calculated as $(-f_n)$ times the log decrement.

From Fig. 8, experimental Curve C, these calculations yield a log decrement of 0.013 (equivalent to a damping ratio of 0.002) and the real part of the complex eigenvalue, λ, = -1.65. Clearly the configuration of Fig. 8 is only marginally stable, as predicted. The fact that the Multiplane Balancing method can balance such a lightly damped rotor is confirmation of the effectiveness of the method under nonideal conditions.

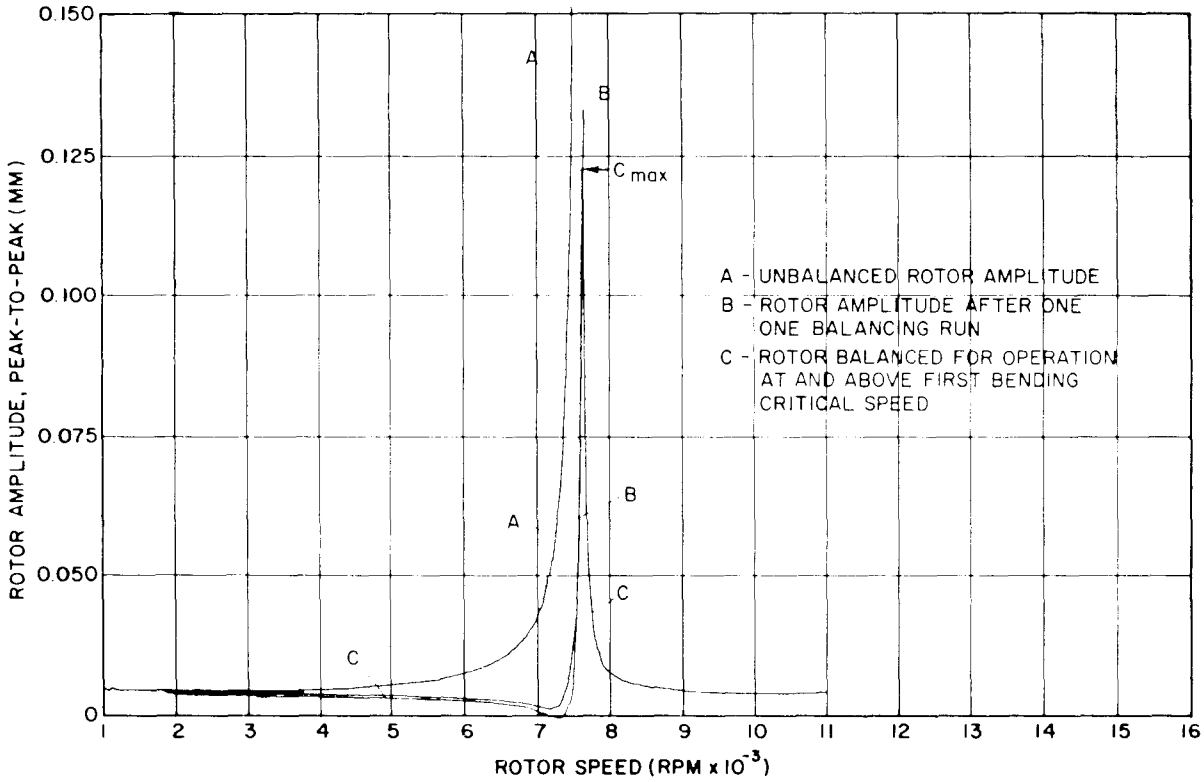

Fig. 8 Vertical rotor amplitudes at shaft center -- initial conditions and after one and two balancing runs by the least squares procedure (four vertical probes, rotor with 4.80 cm dia at flat sections)

Gravitational Excitation

A rotor with unequal stiffness in two axes exhibits a nonsynchronous amplitude increase in the speed region around one-half of the first rotor bending critical speed. This amplitude increase, generally viewed as the result of "gravitational excitation," has been observed for all test cases of the rotor with flat sections at vibrational frequencies corresponding to the first critical speed. The oscilloscope display of the rotor orbit, characterized by a very pronounced inner loop, nearly equal in size to the outer loop, was observed in the rotor orbit display [see Fig. 9(a)].

In its original configuration the test rotor had flat sections with a major diameter of 6.45 cm and heavier end masses weighing 8.6 kg each. The bearing lubricant had a viscosity of 0.65 cS. Under these conditions the rotor exhibited amplitudes at the gravitational excitation frequency which could not be negotiated without endangerment of the instrumentation probes and rotor. When rotor damping was increased through substitution of a bearing fluid with higher viscosity (5 cS), and rotor mode shapes were changed to give relatively larger bearing amplitudes by substitution of lighter rotor end masses (4.94 kg each), rotor amplitudes at the gravitational excitation frequency were reduced substantially. (Increasing the viscosity alone to values up to 65 cS was not sufficient to effect noticeably lower amplitudes.) Typically, the reduced amplitudes did not exceed approximately twice the "background" amplitude values found at slightly higher and lower speeds.

The level of unbalance did not noticeably affect the magnitude of the rotor amplitudes due to gravitational excitation. When one very light rotor end mass of 1.13 kg was substituted for the medium-sized steel mass of 4.94 kg and rotor diameters in the flat sections were progressively reduced, the severity of the gravitational excitation also seemed to decrease accordingly. For the final and stable test condition of the rotor, response to gravitational excitation was insignificant [see Fig. (b)]. It must be noted at this point that the very same rotor before the flats were added to it and operating in low viscosity bearing fluid (0.65 cS) with heavy end masses (8.6 kg each), occasionally exhibited response to gravitational

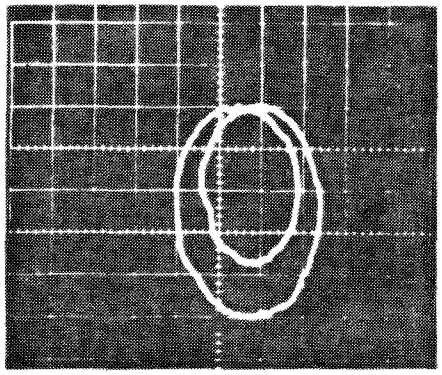

ONE MAJOR DIVISION EQUALS APPROXIMATELY 0.5 MIL - ROTOR SPEED=4470 RPM

Fig. 9(a) Gravitational excitation of rotor with 6.50 cm dia at flat section

excitation. When present, the gravitational excitation was of low to moderately-low severity, but nevertheless had a well-developed inner loop.

CONCLUSIONS

1 The characteristics of a rotor with flexural asymmetry are a noticeable response to gravitational excitation when running at approximately half its first bending critical speed, and a potential for instability when operating between the bending critical speeds associated with its soft and stiff axes.

2 The onset of instability is marked by a sudden rise in amplitude.

3 The unstable vibrations are synchronous with rotational speed.

4 Observation for a three-mass rotor with

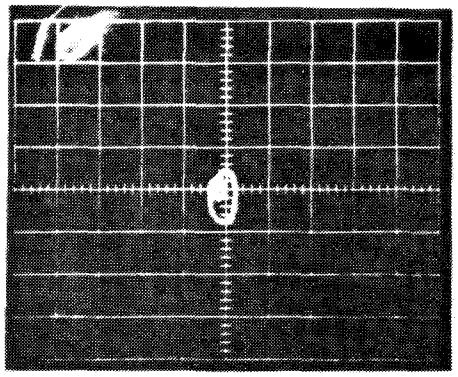

ONE MAJOR DIVISION EQUALS APPROXIMATELY 1.0 MIL - ROTOR SPEED=3850 RPM

Fig. 9(b) Gravitational excitation of rotor with 4.80 cm dia at flat section

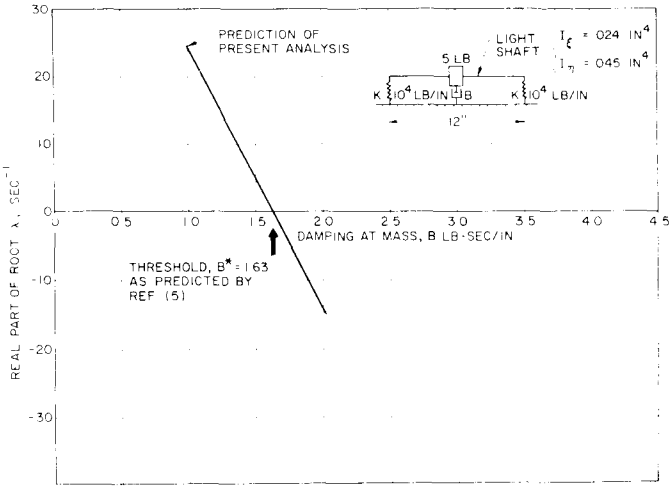

Fig. 10 Check of stability analysis for asymmetric shaft. Comparison with Bones and Hannam (5)

machined flats at a flexible location in the rotor are consistent with predictions of a general purpose analysis developed to account for flexural assymetry in a multi-mass, flexible rotor.

5 The Multiplane-Multispeed Balancing method is able to balance, effectively, a rotor-bearing system whose inferred log decrement, and damping ratio for a bending critical speed, are 0.013 and 0.002, respectively.

ACKNOWLEDGMENTS

The work presented in this paper was sponsored by NASA-Lewis Research Center. The NASA Program Manager was Dr. David P. Fleming. The authors' wish to thank NASA for permission to publish the results of this work.

REFERENCES

1 Smith, D. M., "The Motion of a Rotor Carried by a Flexible Shaft in Flexible Bearings," Proceedings of the Royal Society, 1933, Vol. 142, Series A, p. 92.

2 Foote, W. R., Poritsky, H., and Slade, J. J., Jr., "Critical Speeds of a Rotor With Unequal Shaft Flexibilities Mounted in Bearings of Unequal Flexibility," Journal of Applied Mechanics, Vols. A77, A84, 1943.

3 Hsu, C. S., "On the Parametric Excitation of a Dynamic System Having Multiple Degrees of Freedom," Transactions of ASME, Journal of Applied Mechanics, 1963, Vol. 85, Series E, p. 367.

4 Hsu, C. S., "Further Results on Parametric Excitation of a Dynamic System," Transactions of ASME, Journal of Applied Mechanics, 1965, Vol. 87, Series E, p. 73.

5 Bones, J. A., and Hannam, R. G., "Whirling of Shafts With Asymmetric Stiffness," Journal of Mechanical Engineering Science, Vol. 8, No. 4, 1966, p. 437.

6 Black, H. F., "Parametrically-Excited Lateral Vibrations of an Asymmetric Slender Shaft in Asymmetrically Flexible Bearings," Journal of Mechanical Engineering Science, Vol. 11, No. 1, 1969, p. 57.
57.

7 Lund, J. W., "Stability and Damped Critical Speeds of a Flexible Rotor in Fluid Film Bearings," ASME Paper No. 73-DET-103.

8 Tessarzik, J. M., Badgley, R. H., and Anderson, W. J., "Flexible Rotor Balancing by the Exact Point-Speed Influence Coefficient Method," Transactions of ASME, Journal of Engineering for Industry, Vol. 94, Series B, No. 1, Feb. 1972, p. 148.

9 Tessarzik, J. M., Badgley, R. H., and Fleming, D. P., "Experimental Evaluation of Multiplane-Multispeed Rotor Balancing Through Multiple Critical Speeds," Transactions of ASME, Journal of Engineering for Industry, Vol. 98, Series B, No. 3, Aug. 1976, p. 988.

APPENDIX A

CHECK OF ANALYSIS AGAINST REFERENCES

Fig. 10 illustrates a symmetrical single mass rotor on a light asymmetrically flexible shaft, supported in flexible bearings. The mass is damped by a linear dashpot connected to ground. Bones and Hannam (5) have analyzed this case to yield the required level of damping (B*) for the onset of instability. Their results are reproduced as equation (A-1).

$$\frac{B^*}{2M\omega_o} = \left[\frac{1 - (1-d^2)^{1/2}}{2}\right]^{1/2} \qquad \text{(A-1)}$$

where

$$d = \frac{\left(\omega_2^2 - \omega_1^2\right)}{\left(\omega_1^2 + \omega_2^2\right)} = .1334 \text{ for the rotor of Fig. 10} \qquad \text{(A-2)}$$

$$\omega_1 = \sqrt{K_1^*/M} = 877.9 \text{ rad/sec} \qquad \text{(A-3)}$$

$$\omega_2 = \sqrt{K_2^*/M} = 1004. \text{ rad/sec} \qquad \text{(A-4)}$$

$$K_1^* = 1/\left[\frac{1}{2K} + \frac{L^3}{48EI_s}\right] = 9.983 \times 10^3 \text{ lb/in.} \qquad \text{(A-5)}$$

$$\omega_o = \sqrt{\frac{\omega_1^2 + \omega_2^2}{2}} = 943. \qquad \text{(A-6)}$$

$$K_2^* = 1/\left[\frac{1}{2K} + \frac{L^3}{48EI_r}\right] = 13.06 \times 10^3 \text{ lb/in.} \qquad \text{(A-7)}$$

So that B* for the rotor of Fig. 10 is 1.63. The analysis developed in the present paper can be used to establish this threshold condition by plotting the real part (λ) of the complex eigenvalue versus damping, and seeking the value of B* at which $\lambda = 0$. This has been done in Fig. 10 and the resultant value of damping is 1.63, as predicted by Reference (5).